applied sciences

MDPI

Article

Evaluation of Green Synthesis (*Withania somnifera*) of Selenium Nanoparticles to Reduce Sperm DNA Fragmentation Diabetic Mice Induced with Streptozotocin

Iman A. Mohammed Ali [1], Hazim Ismail AL-Ahmed [2] and Ali Ben Ahmed [1,*]

[1] Laboratory of Applied Physic, Faculty of Sciences of Sfax, University of Sfax, Sfax 3000, Tunisia
[2] Biotechnology Research Center, University of Al-Nahrain, Baghdad 64074, Iraq
* Correspondence: ali.benahmed@isbs.usf.tn

Abstract: Given the promising good future of selenium nanoparticles in the modern field of health, selenium nanoparticles have played an important role in increasing sperm efficacy and antioxidant defense mechanisms. In the present study, we synthesized the selenium nanoparticles (Se NPs) in a safe and harmless medical manner from the aqueous extract of *Withania somnifera* roots. The formation of Se NPs was confirmed using different techniques of spectroscopy. The results showed a broad absorption peak of up to 622 nm of wavelength. With clumps of NPs forming what looks like a porous structure, excellent uniform spherical shape of Se NPs and distribution behavior with the least aggregation, it appears as an average single particle size of around 22 nm. Secondly, we evaluated their potential improvement functions on the antioxidant enzyme and DNA damage of sperm induced by STZ-induced diabetes in mice. Additionally, antioxidant drugs and natural male cell therapy were also studied. Fifty male experimental mice with an average weight (23–30 kg) were divided into five groups and fed once daily with IP, streptozotocin, metformin, streptozotocin with Se NPs and later streptozotocin with Se NPs for 35 days. Se NPs treatment increased antioxidant enzyme activities and improved sperm quality in STZ-induced diabetic mice by stabilizing the level of reactive oxygen species. Green synthesis appears to be a safe method for producing selenium nanoparticles, and Se NPs are more beneficial than inorganic and organic selenium.

Keywords: green synthesis; selenium nanoparticles; spectroscopies characterizations; comet assay; DNA fragmentation

Citation: Mohammed Ali, I.A.; AL-Ahmed, H.I.; Ben Ahmed, A. Evaluation of Green Synthesis (*Withania somnifera*) of Selenium Nanoparticles to Reduce Sperm DNA Fragmentation Diabetic Mice Induced with Streptozotocin. *Appl. Sci.* **2023**, *13*, 728. https://doi.org/10.3390/app13020728

Academic Editor: Marco G. Alves

Received: 30 November 2022
Revised: 21 December 2022
Accepted: 26 December 2022
Published: 4 January 2023

1. Introduction

Recently, it has been noted that plants are crucial in the creation of different types of nanoparticles, including silver, gold, zinc, selenium and others [1,2], which in turn were used as a means to deliver medicine to the affected part of the patient, through the characteristic possessed by nanoparticles; the greater the area of the particle, the smaller its size. This increases its ability to penetrate deeper into the living body [2]. The concept of discovery and development of nanomedicines and methods of their delivery opened a wide field in modern treatment [3]. Among the nanomaterials used in therapeutic applications were selenium nanoparticles. Selenium is an important and essential element of the elements that affect the physiological functions and the health of the human body. It is considered a very important transporter of drugs to the affected organ, as it showed its effectiveness against oxidation, free radicals, anti-bacteria and others [4–6]. Selenium nanoparticles can play a key and important role in many metabolic pathways and regulate the physiological functions of the organism [7], as it enters the metabolism of thyroid hormone and acts as an antioxidant and fights free radicals resulting from a disease or a particular cause, as well as maintaining the functions of the immune system and the fight against cancer cells. Through the study published by Cláudio Ferro et al. [8], it was proven that selenium nanoparticles are very effective in combating the weakness and deformation

of the sperm as a result of chronic disease, where an improvement in sperm production and good qualities was observed in addition to other uses. The daily amount that the body needs from selenium can be obtained by eating some foods containing this element, including vegetables, grains, mushrooms and other sources such as medicines [9]. The best way to produce nanoscale selenium with less toxicity and good biological activity compared to organic and inorganic selenium compounds is to use different reducing agents [10], including ascorbic acid and different plant sources. The plant *Withania somnifera* is a very important source that can be used in the manufacture of nanoparticles due to the active substances it contains [1]. This herb, in addition to ascorbic acid, can be used together in the synthesis of nanoparticles, where it was found that the two substances have an effective role in stimulating the immune system in the body of the organism, and it has a great role against the toxicity of metals transported in the water [11].

In this paper, we present for the first time all experimental results related to the green production of selenium nanoparticles and nanostructure characterization by XRD spectroscopy, and the crystallite size was estimated using the Scherer equation. The morphological analysis was examined by using Scanning Electronic Microscopy (SEM) and Transmission Electronic Microscopy (TEM). UV-Visible Spectroscopy was utilized to explore the absorption region of the synthesis nanoparticles, and according to the Tauc method, the energy band gap was estimated. On the other hand, the method of spinal dislocation was used to isolate sperm from the testes of male mice, according to what was stated in the study [12]. Next, the samples were prepared for comet examination [13]. All results obtained were analyzed, interpreted, discussed and compared with similar works in the literature.

To our knowledge, no papers have reported the green synthesis of Se NPs from the roots of *Withania somnifera*, nanostructure properties, morphological analysis, linear optical properties, protective biological activity against DNA damage from induced diabetes mellitus and a comet assay. For sperm, the effect of nanoparticles in the treatment of toxicity resulting from reactive oxygen species was studied.

2. Materials and Methods

2.1. Preparation of Selenium Nanoparticles

The roots of the plant *Withania somnifera* were obtained from the market in Baghdad, and it was categorized by the herbalist at the College of Science/University of Baghdad, where it was found that this plant belongs to the nightshade family. The plant extract was prepared from deionized water after the roots were washed several times with distilled water and dried for 24 h, after which the roots of the plant were ground using an ordinary mill.

The plant extract was prepared by stirring for 10 min at 40–45 °C, filtered using Whatman n°1 filter paper and then centrifuged for 15 min. It was filtered by taking only the supernatant (Figure 1). An amount of 10 mL of plant extract and 0.14 g of 100 mL of selenious acid were mixed with continuous stirring using a magnetic stirrer (600 rpm) at 40–45 °C for 15 min. Then, 10 mL of ascorbic acid was added to the solution by pipette at 40–45 °C for 30 min until the color of the solution turned reddish-orange. The solution was allowed to cool, and then a small portion (1 mL) of the solution was used for UV analysis. The precipitate is then separated by a centrifuge and rinsed with water and ethanol several times. The precipitate was dried in an oven at 100 °C for 4 h. As can be shown in Figure 1, the red Se NPs particles were suspended in PBS solution to preserve them until use. The preparation was carried out according to references [14–16] with some modifications (see next paragraph).

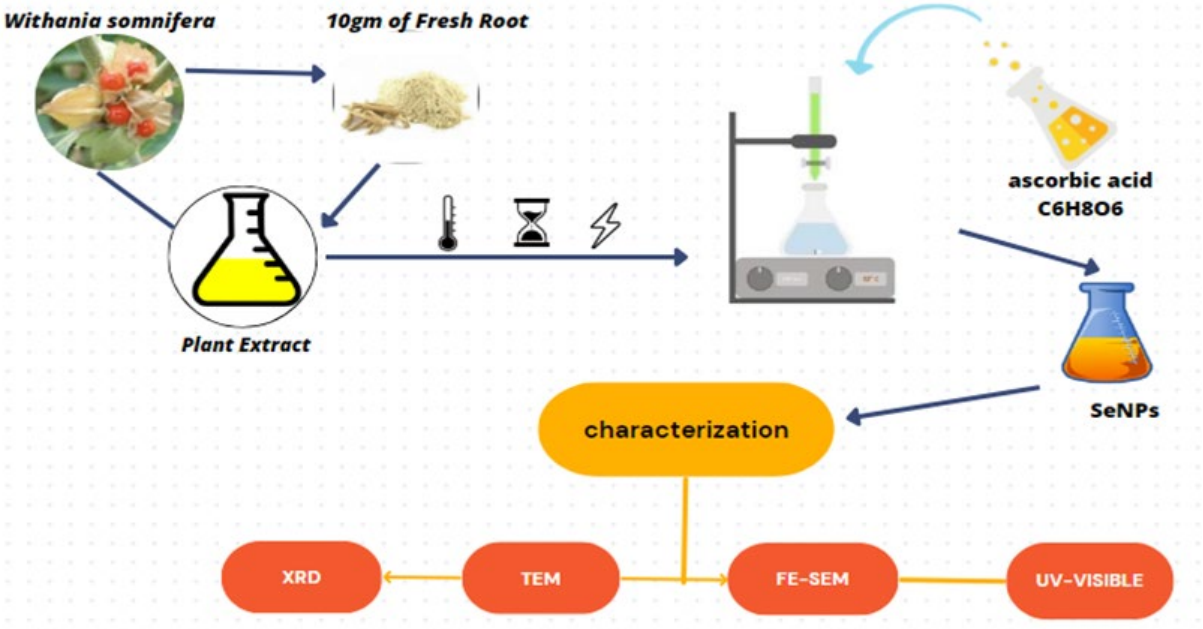

Figure 1. Steps of green synthesis method of silver nanoparticles using *Withania somnifera* extract.

2.2. Parameters Used to Study the Characterization of Nanoparticles

2.2.1. XRD Analysis

The size and purity of the nanoparticles were characterized. The X-ray diffraction pattern was assessed using a Cu Ka-powered Philips Panlytical X'pert Pro X-ray diffractometer with a wavelength of 1.54059 Å. The crystallite size was deduced using the Scherrer equation. The company is Panalytical XPert Pr/UK Origin.

2.2.2. FESEM-Imaging

The structure of the selenium nanoparticles was studied from the size and shape of the nanoparticles using a surface-scanning electron microscope for field emission with a precision of 500 nm operating at 10 kV. It was observed through EDX the appearance of the nano-selenium element in pure and high proportion, according to the device used for examination type in Germany. The company is EDS-Mappin-Line-EBSD.

2.2.3. TEM Analysis

The structure and shape of the nanoparticles were studied using a transmission electron microscope type TEM Instrument ZEISS LE0912 AB/Germany, where an image of the selenium nanoparticles was recorded based on the electron microscopic image formed.

2.2.4. UV-Visible Spectroscopy

The bioreduction in selenium acid was characterized by measuring the wavelength shown in the Shimadzu 2550 UV-Vis spectrophotometer, where a gradual rise in the absorption spectrum was observed until it reached a peak at the scanning range of the samples between 250 and 1000 nm at a scanning speed of 1.856 nm/min. The company is Shimadzu-2450/Japan Origin.

2.3. Animals of Study

Fifty healthy, mature, white male mice weighing range about 23–30 g and aged about 1.5–2.5 months were purchased from the Biotechnology Research Center/Al-Nahrain University. All animals were kept in standard conditions of 22 ± 3 °C with a 12 h light–dark and 12 h light exposure cycle and in a controlled environment. The fifty mice were randomly divided into five groups of ten animals each.

Group 1: This group served as a negative control as mice received normal saline by IP for 35 days;

Group 2: This group was a positive control for STZ (50 mg/kg body weight/day);

Group 3: Diabetic rats of this group were treated with standard metformin (200 mg/kg body weight/day) orally for 35 days;

Group 4: Diabetic rats in this group were treated with selenium particles (200 mg/kg body weight/day) orally for 35 days;

Group 5: Diabetic rats in this group were treated with selenium nanoparticles (2 mg/kg body weight/day) orally for 35 days.

2.4. Sample Preparation for Comet Assay

In this research, an easy method was used to isolate semen from the testes of male mice using the spinal dislocation method. Mice were sacrificed using the method indicated in [17]. The mice were fixed on a dissection board, and the animal's abdomen was washed with ethanol. A central and vertical incision was made using forceps and scissors. The caudal epididymis was cut and placed in a small container containing 2 mL of PBS and carefully mashed using laboratory scissors. A drop of semen was taken and placed on a clean, dry slide, then 3 drops of eosin spot were mixed and spread with another slide and left until microscopy [18].

Slides were prepared 24 h before removal. A total of 250 µL of LM agarose wax made by Cambrex/bioscience of USA origin was dissolved in Eppendorf at a temperature of 100 °C and then placed in a water bath at a moderate temperature of 37 °C. Additionally, 10 µL of sperm cells were taken and added to the agarose wax, and 50 µL of the mixture (cells + agarose) was taken and placed on the glass slides. The slides were placed on ice to ensure that the agarose was not broken while lifting the lid. The slides were placed in two solutions, Trouble G (cell lysis). It is the solution responsible for analyzing and decomposing cells removing membranes and proteins attached to DNA pH > 13 (200 mM NaOH, 1 mM EDTA, left for at least 24 h. After that, the slides were taken and placed in the second solution responsible for drawing a comet that represents pH > 13 (200 mM NaOH, 1 mM EDTA) manufactured by Sigma/Aldrich of USA origin, in sequence (500 mL was set for 30 min). Then the transfer of the damaged DNA begins and extends towards the anode at 40 V and 60 min. The amount of displacement between the tail compared to its head can be considered a measure of the level of DNA damage [19–21]. DNA migration and image drawing were studied using the comet score program [22], and tail length (px), tail DNA (%) and tail mean moment were studied according to the following study [23,24].

2.5. Superoxide Dismutase Assay

Sample preparation is detected for serum or plasma parameters according to the commercial kit Cohesion/China, and the measurement conditions were prepared according to the protocol of the kit manufacturer and as shown in the following Table 1.

Table 1. The protocol of the kit manufacturer.

Reagent (µL)	Sample	Standard	Blank
Reaction Buffer	30	30	30
Substrate	100	100	100
Enzyme	1	1	1
Sample	19	–	–
Standard	–	19	–
Distilled water	–	–	19
Dye Reagent	50	50	50
Mix, stand at room temperature for 30 min, record absorbance measured at 560 nm			

The calculation according to the number of cells or bacteria was recorded by the following equation:

$$\begin{aligned} SOD(U/104) &= (C_{Standard} \times V_{Standard}) \times (OD_{Blank} \\ &\quad -OD_{Sample}) / (OD_{Blank} \\ &\quad -OD_{Standard}) / \left(V_{Sample} \times N / V_{Assay}\right) \\ &= 30 \times \left(OD_{Blank} - OD_{Sample}\right) / (OD_{Blank} \\ &\quad -OD_{Standard}) / N) \end{aligned} \quad (1)$$

where $C_{Protein}$ is the protein concentration (mg/mL); $C_{Standard}$ is the standard activity (30 U/mL); W is the weight of sample (g); $V_{Standard}$ is the volume of standard (0.019 mL); V_{Sample} is the volume of sample (0.019 mL); V_{Assay} is the volume of assay buffer (1 mL); and N is the number of cells or bacteria $\left(N \times 10^4\right)$.

2.6. Statistical Analysis

The results were subjected to statistical analysis using Windows SPSS Vision18 Statistical software; sample methods were evaluated using the ANOVA test, and mean (mean ± SD) were found. p values of $p \leq 0.05$ were considered great.

3. Results and Discussion

3.1. XRD-Analysis

The atomic arrangement, lattice characteristics and crystalline size can all be determined using the crucial method of X-ray diffraction [25].

Figure 2 shows the XRD pattern of the synthesis of selenium nanoparticles (Se NPs); the XRD pattern shows multi peaks with different intensities at 23.4°, 29.6°, 41.2°, 43.5°, 45.3°, 51.6°, 55.8°, 61.5° and 65.1°, which correspond to planes (100), (101), (110), (102), (111), (201), (003), (022) and (210), respectively. This behavior refers to Se NPs and full agreement with JCPDS (01-073-0465); our result is in good agreement with the published result by Cittrarasu et al. in 2021 [26]. The high crystallinity is very clear, and the phase structure of nanoparticles is hexagonal.

The average crystalline size (D) of Se NPs was calculated from Bragg reflections of full width half maximum (FWHM) by Debye–Scherrer equation [27].

$$\mathrm{D} = \frac{0.9\lambda}{\beta \cos \theta} \quad (2)$$

where $\lambda = 1.5406$ is the wavelength of the X-ray and β is the full width half maximum (FWHM) of the peak in radians, and θ is the Bragg angle.

The average crystallite size of nanoparticles (D) is equal to 24.97 nm. The crystallite size of Se NPs is shown in Table 2.

Table 2. The crystallite size of Se NPs.

Sample	**2θ** (°)	**hkl**	**FWHM**(°)	**2θ** (**Rad**)	**FWHM** (**Rad**)	**D** (**nm**)
Se NPs	23.4289	(100)	0.2362	0.204	0.004	34.336
	29.6254	(101)	0.1968	0.259	0.003	41.739
	41.2558	(110)	0.3149	0.360	0.005	26.946
	43.5642	(102)	0.2362	0.380	0.004	36.206
	45.3221	(111)	0.3936	0.396	0.007	21.864
	51.6654	(201)	0.3149	0.451	0.005	28.018
	55.8639	(003)	0.9446	0.488	0.016	9.515
	61.5571	(022)	0.9446	0.537	0.016	9.785
	65.1915	(210)	0.576	0.569	0.010	16.364
Average crystallite size (nm)						24.97

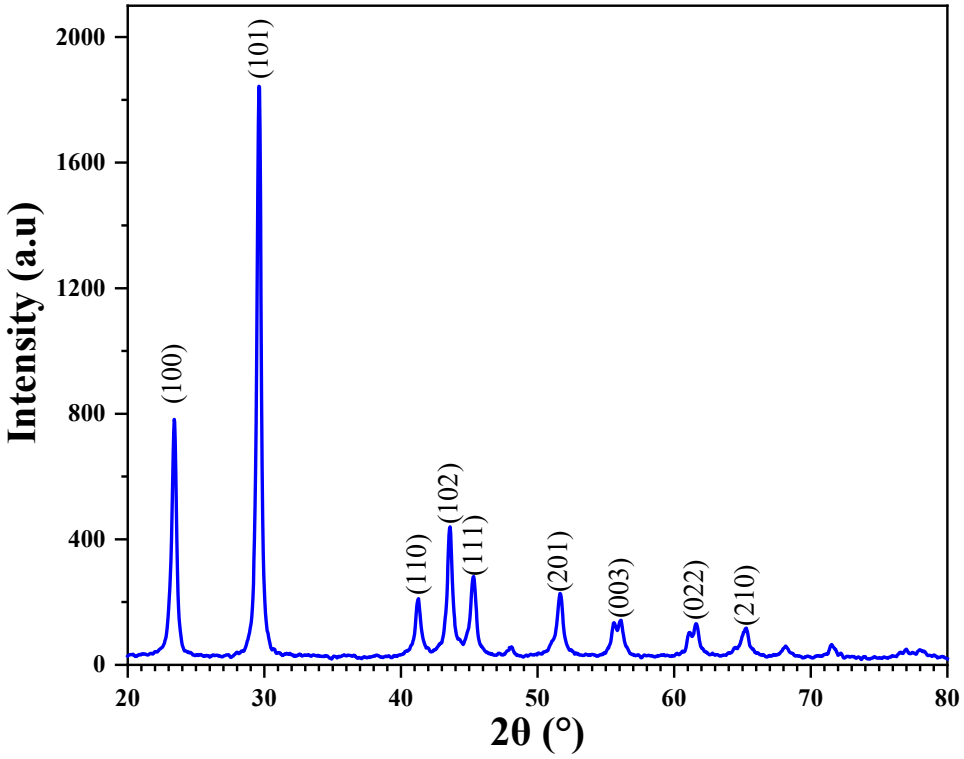

Figure 2. XRD pattern of synthesized Se NPs.

3.2. FESEM Analysis

Field emission scanning electron microscopy (FESESM) provides the ability to study the topography of the surfaces of nanomaterials and determine their applicability in different fields. Figure 3 shows the morphology of the synthesis of Se NPs. From the figure, the results confirm the presence of clumps of nanoparticles, which form what looks like a porous structure. It is widely known that surface plasmon resonance causes spherical nanoparticles to have a characteristic optical absorption peak of about 1.5 keV. A similar result was published by Alagesan et al. in 2019 [28].

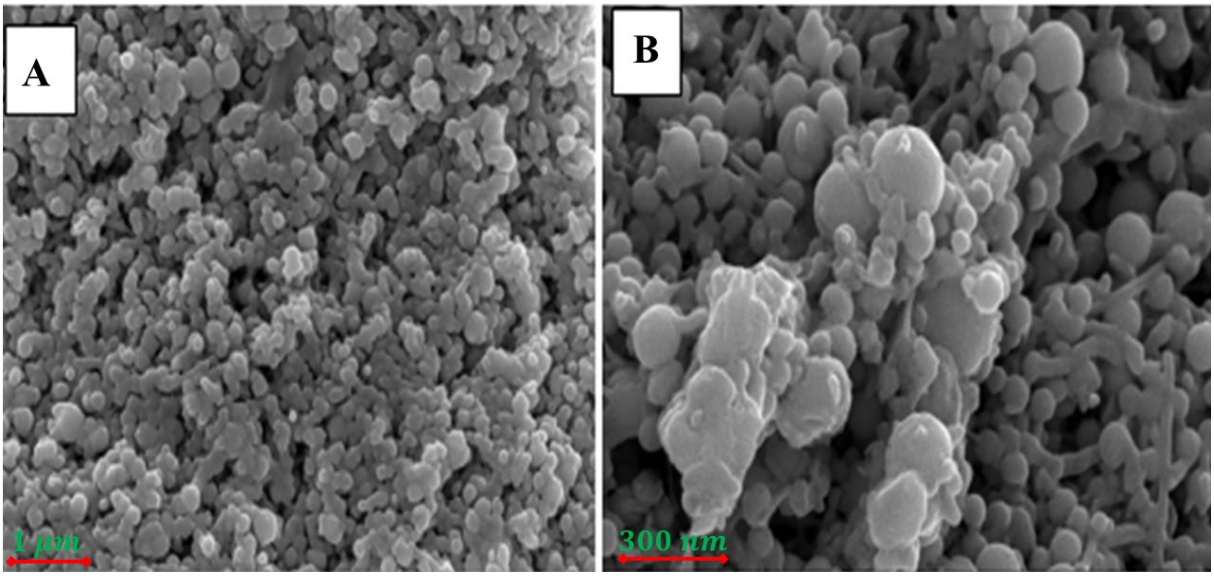

Figure 3. FE-SEM images of Se NPs synthesized at (**A**) 1 µm and (**B**) 300 nm using *Withania somnifera* extract.

3.3. TEM Analysis

TEM is one of the cutting-edge analytical measurement technologies used to image and analyze nanoparticles to determine their size and shape [15]. Figure 4A,B show the TEM image of Se NPs prepared by the green synthesis method. The images show nanoparticles are an excellent uniform spherical shape of Se NPs and the distribution behavior with less aggregation, therefore, shown as an individual particle. Figure 4C explains the histogram size distribution on Se NPs, and the average size is about 22 nm. This result is in good agreement with the crystallite size determined from XRD analysis. A similar result is published by Galić et al. in 2022 [29].

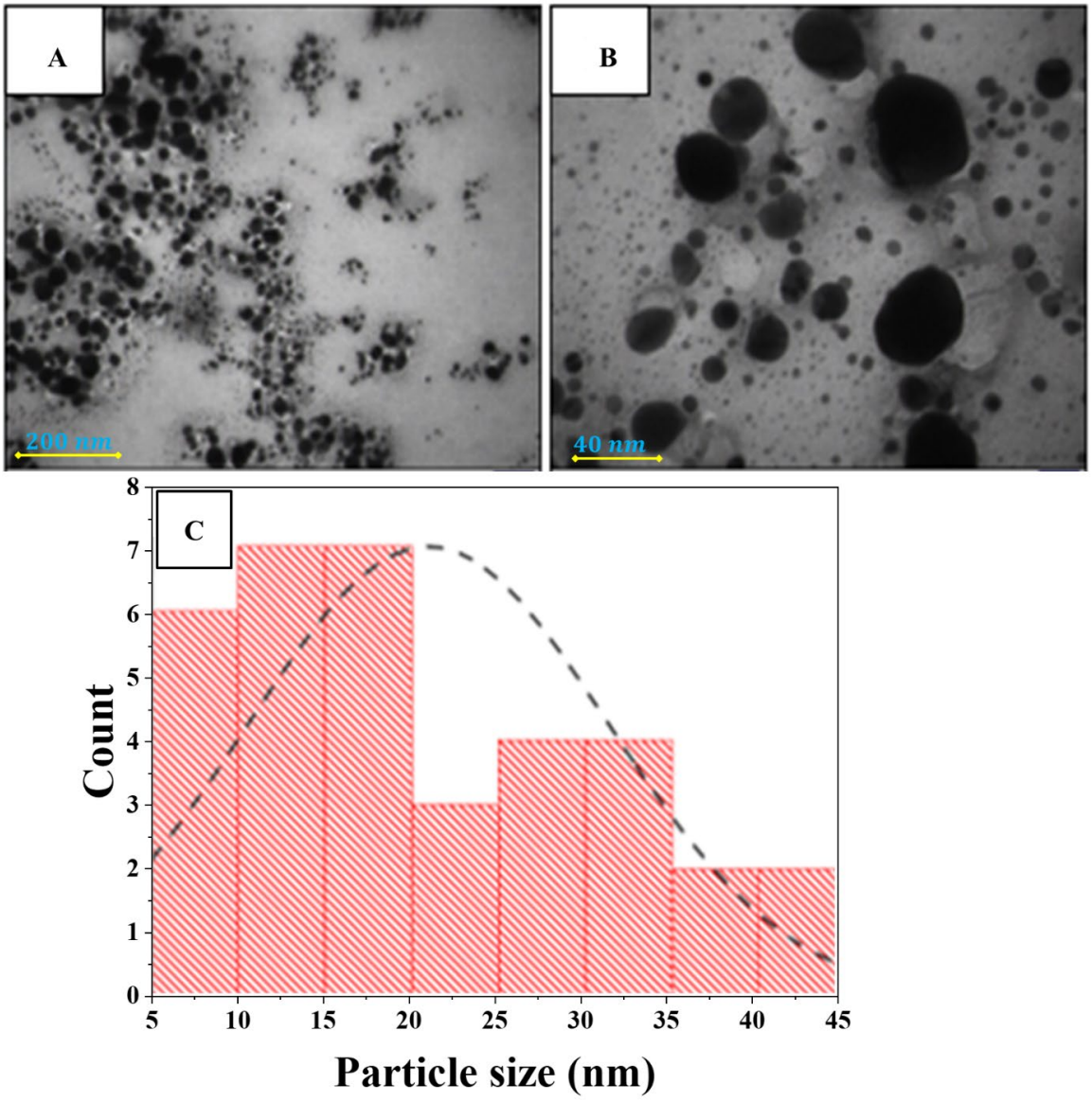

Figure 4. TEM images of Se NPs synthesized at (**A**) 200 nm magnification, (**B**) 40 nm magnification and (**C**) the histogram size distribution using *Withania somnifera* extract.

3.4. Optical Properties

The UV-Visible absorption spectrum displayed in Figure 5 show the electromagnetic radiation absorbed by Se NPs. The results confirm the existence of two absorption bands centered at the wavelength of $\lambda_1 = 458$ nm and $\lambda_2 = 622$ nm. The middle band centered at $\lambda_1 = 458$ nm is related to selenium nanoparticles, while the strong band centered at $\lambda_2 = 622$ nm can be attributed to surface plasmonic resonance and the small size of

nanoparticles prepared by the synthesis process. Our result is consistent with the results of the work published in 2020 and 2018 by Ahmed et al. and Pouri et al., respectively [30,31].

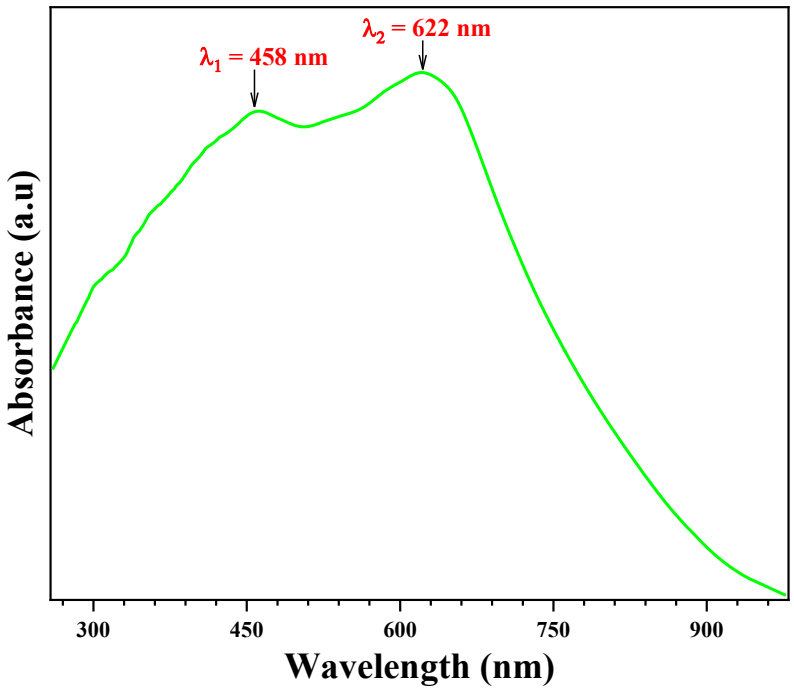

Figure 5. UV-visible absorbance spectra of Se NPs.

Figure 6 indicates the relation between the optical absorption coefficient and the wavelength of Se NPs prepared by the green method. The results confirm that the sample has high absorption coefficient values in the visible region, reaching its peak at the wavelength $\lambda_2 = 622$ nm. The current results are consistent with the results of the works published in 2013 by Habubi et al. and in 2019 et al. by Panchal [32,33].

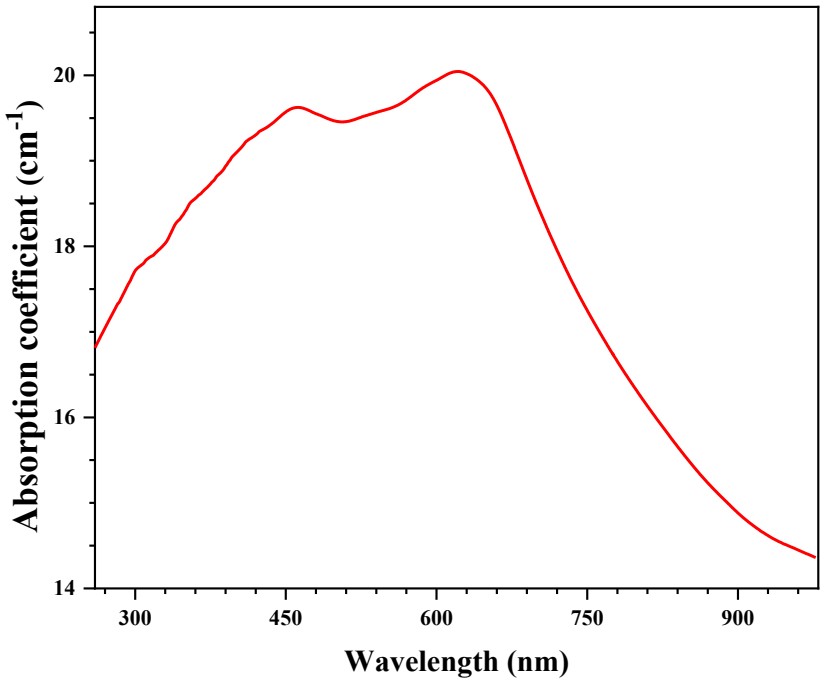

Figure 6. Absorption coefficient as function of wavelength of synthesized Se NPs.

The dependence of the optical absorption coefficient with the photon energy helps to study the band structure and the type of transition of electrons. By using the absorption data, the optical absorption coefficient (α) can be deduced by applying Beer–Lambert's law [34]:

$$\alpha = \frac{2.3030 \times A}{e} \tag{3}$$

where A is the maximum absorbance, and e is the sample thickness $(e = 0.003\ \text{cm})$.

The inter-band absorption theory shows that the absorption coefficient near the threshold versus incident energy is given by the following Pankove's relation [35]:

$$\alpha h\nu = B\left(h\nu - E_g\right)^n \tag{4}$$

where B is the probability parameter for the transition and E_g the optical gap energy. For allowed direct transitions, the coefficient n is equal to $\frac{1}{2}$, and for indirect allowed transitions, $n = 2$. Due to the direct band gap, the compound under study has an absorption coefficient (α) obeying the following relation for high photon energies $(h\nu)$:

$$\alpha h\nu = B\left(h\nu - E_g\right)^{\frac{1}{2}} \tag{5}$$

The E_g value corresponding to direct band gap transitions (see Figure 7) can be calculated via the $(\alpha h\nu)^2$ versus $h\nu$ by using the following formula:

$$(\alpha h\nu)^2 = B\left(h\nu - E_g\right) \tag{6}$$

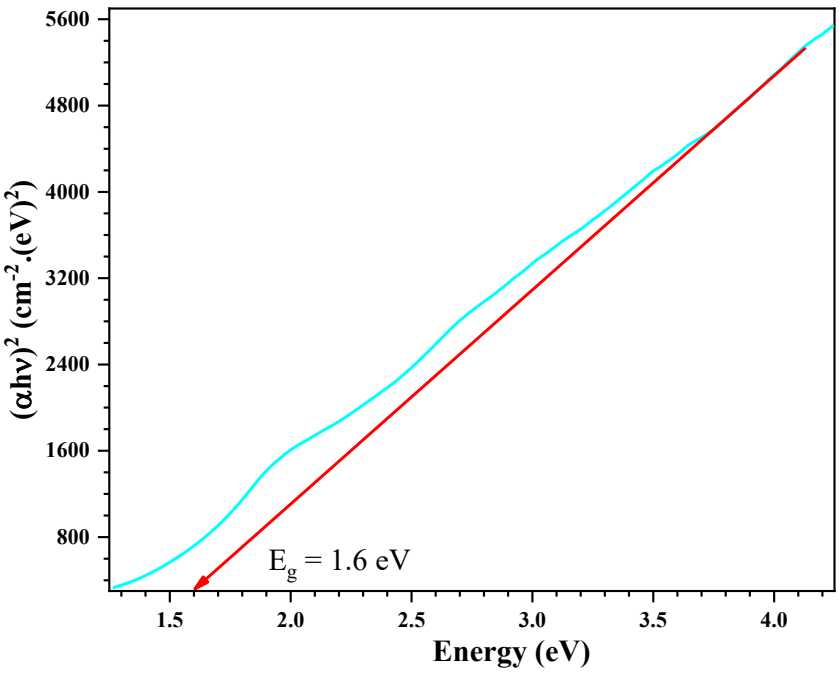

Figure 7. Tauc plot of prepared Se NPs.

The values of E_g were estimated from the intersection of the extrapolated linear part of the $(\alpha h\nu)^2$ curves with the energy axis. Figure 7 shows the variation in $(\alpha h\nu)^2$ versus $h\nu$ before and after irradiation with laser beams for Se NPs. The results confirm that the energy gap was approximately 1.6 eV. The present results are consistent with the authors' findings [36,37].

3.5. Alkaline Comet Assay

The results showed a protective effect against the DNA degradation activities caused by STZ-induced diabetes, and the results of the single-cell gel electrophoresis test revealed that the SeNPs overcome the cytotoxicity and cause less sperm cell death by reducing the percentage of damage. The results presented in Figures 8–10 indicate that there are statistically significant differences between all the treated groups, and the most effective treatment was in reducing the rates of DNA damage and restoring the concentration and normal shape of sperm in the testicles of diabetic mice compared to the control group.

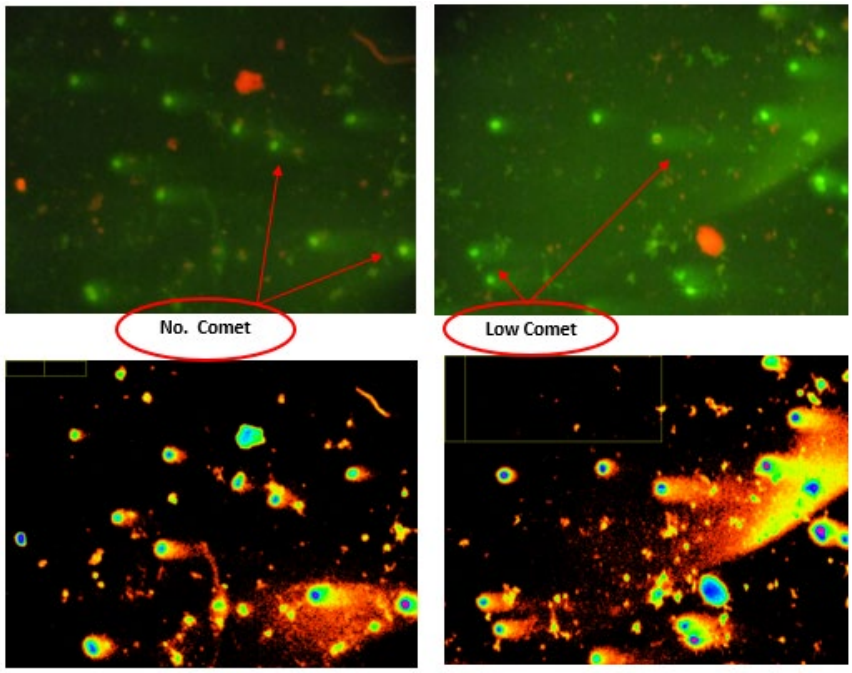

Figure 8. Treated group with Se NPs: high numbers of cells with no comet and low comet by using comet score program.

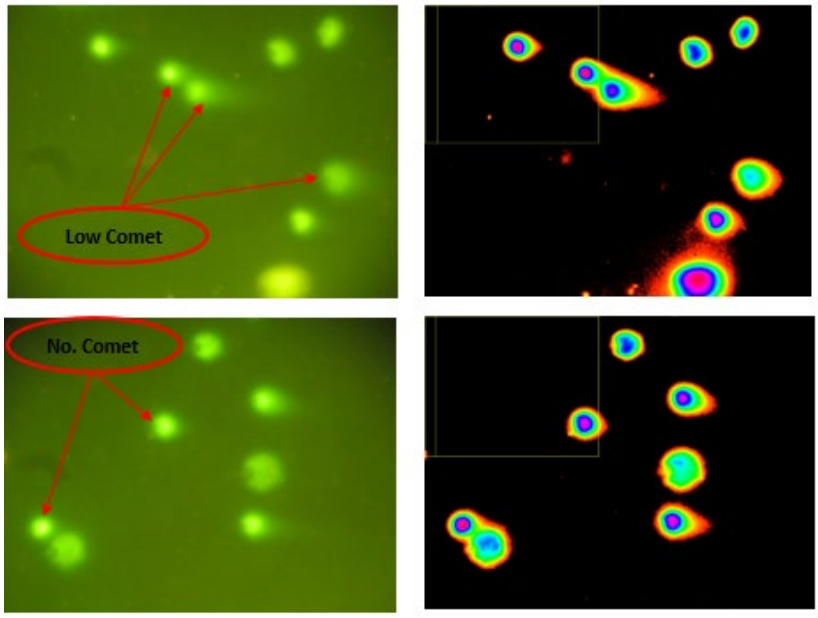

Figure 9. Control group (negative): high numbers of cells with low comet and no comet by using comet score program.

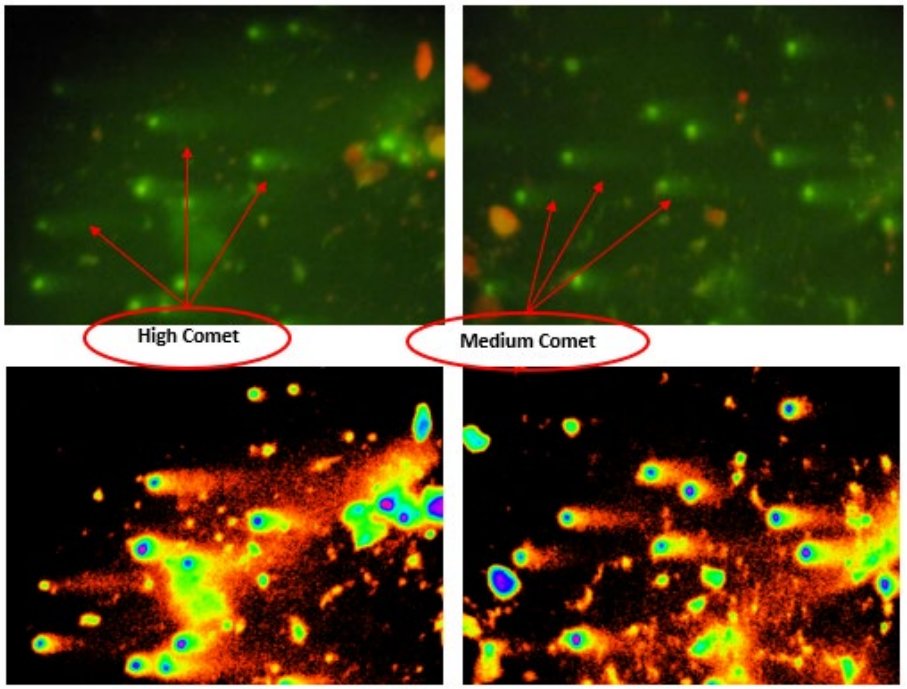

Figure 10. Positive control group (DM): high numbers of cells with high comet and medium comet by using comet score program.

Table 3 shows that treatment with nanoselenium led to a significant improvement ($p \leq 0.05$) in the value of the medium and high damage, as the value decreased significantly compared to the streptozotocin group.

Table 3. The result of the comet assay in sperm after treatment with SeNPs.

Parameters Groups	No Damage % (Mean ± SD)	Low Damage % (Mean ± SD)	Medium Damage % (Mean ± SD)	High Damage % (Mean ± SD)
Neg. control	A42.478 ± 0.975	A43.41 ± 0.553	D7.066 ± 0.942	D7.045 ± 0.599
STZ	D33.189 ± 1.565	D33.698 ± 0.878	A15.025 ± 0.554	A18.088 ± 1.072
STZ + Met	C37.909 ± 0.856	C38.37 ± 0.878	B10.852 ± 0.557	B12.869 ± 0.329
STZ + Se	BC38.681 ± 1.33	C38.487 ± 0.939	BC10.484 ± 0.613	B12.347 ± 1.693
STZ + Se NPs	B39.705 ± 0.406	B40.087 ± 0.724	C9.487 ± 0.605	C10.721 ± 0.712
LSD	1.659583	1.215511	1.010036	1.505262
p-value	0.00075	0.00008	0.00006	0.00047

- STZ = streptozotocin diabetic mice
- Met = metformin
- Different capital and small latter represent significant $p \leq 0.05$.
- LSD: least significant difference.
- *p* value: probability value.

The results also showed the parameters of tail length (px), tail DNA (%) and tail mean moment according to Table 4. The qualitative mean value of the SeNPs marked with the letter D is not significantly different from the control sample, but the qualitative mean values of STZ are different. Additionally, those marked with the letter A were significantly different from the negative control group ($p \leq 0.05$). On the other hand, the percentage of DNA was studied to evaluate the integrity of sperm. We conclude that the synthesis of SeNPs in this way is beneficial in DNA healing by reducing or eliminating oxidative stress in the immune system, thus preventing ROS from stimulating lipid peroxidation responsible for subsequent DNA damage. Hence the stability of energy metabolism [38] and

this result agrees with the previous study by El-Nekeety et al. and Artemani et al. [39,40]. Treatment with SeNPs alone was more effective than either MET or Se use.

Table 4. Measurement of the tail length, tail DNA percentage and tail moment by using comet score program.

Parameters Groups	Comet Score Program (Mean ± SD)		
	Tail Length (px)	**Tail DNA (%)**	**Tail Mean Moment**
Neg. control	D65.044 + 8.035	D0.0246 + 0.00089	E0.000231 + 0.0000521
STZ	A303.775 + 24.336	A12.114 + 2.007	A7.3351 + 2.155
STZ + Met	C90.261 + 11.074	B4.125 + 1.008	B4.224 + 1.007
STZ + Se	B105.752 + 13.276	B4.026 + 0.986	C2.965 + 0.8112
STZ + Se NPs	D75.842 + 8.117	C2.243 + 0.411	D1.7775 + 0.477
p-Value	0.000431	0.000512	0.000116

- STZ = streptozotocin diabetic mice
- Met = metformin
- Different capital and small latter represent significant $p \leq 0.05$.
- LSD: least significant difference.
- *p* value: probability value.

3.6. Super Oxide Dismutase Level on Control and Treated Groups (SOD)

The values from the results presented in Table 5 can be seen. The SOD level was $4.763 + 0.480$ units/mg in the control group; this value decreased significantly ($p \leq 0.05$) in the Streptozotocin group $1.673 + 0.205$ units/mg, while in both groups that were treated with metformin and selenium extract, it rose at the same level, which was $2.321 + 0.399$ units/mg and $2.128 + 0.166$ units/mg, respectively.

Table 5. The result of the SOD after treatment with SeNPs.

Parameters	SOD U/mg (Mean ± SD)
Neg. control	A4.763 + 0.480
STZ	D1.673 + 0.205
STZ + Met	C2.321 + 0.399
STZ + Se	CD2.128 + 0.166
STZ + Se NPs	B2.917 + 0.234
LSD	0.482896
p-value	0.00040

- STZ = streptozotocin diabetic mice
- Met = metformin
- Different capital and small latter represent significant $p \leq 0.05$.
- LSD: least significant difference.
- *p* value: probability value.

The green SeNPs group showed the best result, which was $2.917 + 0.234$, and these results showed a significant increase ($p \leq 0.05$) in the level of SOD compared to DM. Additionally, as shown in Figure 11, the group indicates its excessive use in mitigating free radicals I born during DM. This note has already been reported in animals with diabetes [41].

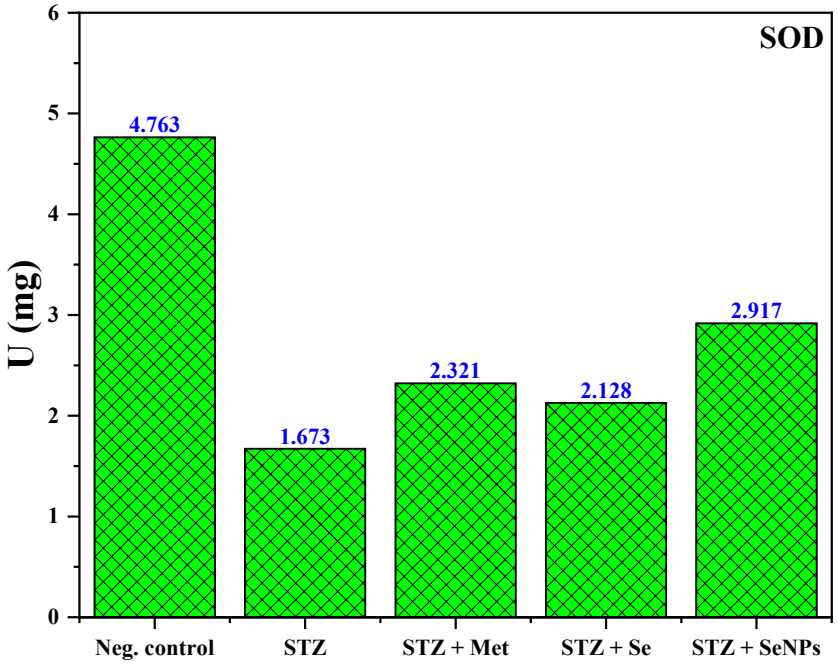

Figure 11. Super oxide dismutase level on control and treated groups.

The effect of SeNPs on plasma oxidative enzymes and their increased activity is an indication of their presence and the ability to search for reactive oxygen species, thus contributing to the protective effect against oxidative stress and preventing further damage to membrane lipids [42].

4. Conclusions

Se NPs were successfully synthesized by the green synthesis method. The hexagonal crystalline structure and the morphological properties were confirmed by experimental techniques. The average nanoparticle size is equal to 22 nm. The bandgap energy (1.6 eV) for Se NPs presented a good agreement compared to the standard behavior of Se NPs. Analysis of the biological activity of Se NPs was achieved using single-cell gel electrophoresis (comet assay). It was found that there was a significant decrease in the amount of DNA damage and weakness after administering doses to diabetic mice with selenium NPs. The current study revealed that even small amounts of Se NPs administered into the bloodstream have an effective effect on living cells, where nanoparticles can significantly improve the characteristics and parameters of semen through their antioxidant properties. Additionally, it has a protective effect against the death of sperm cells and thus helps them reduce the percentage of damaged and distorted cells and increase the percentage of active, healthy sex cells. Therefore, it is recommended to synthesize nanoparticles and use them as a therapeutic option to reduce infertility caused by diabetes.

Author Contributions: Conceptualization, I.A.M.A.; methodology, I.A.M.A.; validation, H.I.A.-A.; formal analysis, H.I.A.-A.; investigation, A.B.A.; data curation, I.A.M.A. and A.B.A.; writing—original draft preparation, I.A.M.A. and A.B.A.; writing—review and editing, I.A.M.A. and A.B.A. All authors have read and agreed to the published version of the manuscript.

Funding: This research received no external funding.

Institutional Review Board Statement: Not applicable.

Informed Consent Statement: All methods were carried out in accordance with relevant guidelines and regulations. (1) All experimental protocols were approved by the ethics committee in the Biotechnology research center at the University of Al-Nahrain, Baghdad 35095 Iraq: Application number 60, Reference number 21-3, date 20 May 2022. (2) All methods are reported in accordance

with ARRIVE guidelines for the reporting of animal experiments. (See attached file: "Research Ethics Checklist (Animals)").

Data Availability Statement: All data generated or analyzed during this study are included in this published article. The data that support the findings of this study are available from the corresponding author, (Ali Ben Ahmed: ali.benahmed@isbs.usf.tn), upon reasonable request.

Acknowledgments: We thank all members of the Biotechnology research center at the University of Al-Nahrain for their assistance with the biologic part.

Conflicts of Interest: The authors declare no conflict of interest.

References

1. Kiani, B.H.; Haq, I.-u.; Alhodaib, A.; Basheer, S.; Fatima, H.; Naz, I.; Ur-Rehman, T. Comparative Evaluation of Biomedical Applications of Zinc Nanoparticles Synthesized by Using *Withania somnifera* Plant Extracts. *Plants* **2022**, *11*, 1525. [CrossRef] [PubMed]
2. Pyrzynska, K.; Sentkowska, A. Biosynthesis of selenium nanoparticles using plant extracts. *J. Nanostruct. Chem.* **2022**, *12*, 467–480. [CrossRef]
3. Đorđević, S.; Gonzalez, M.M.; Conejos-Sánchez, I.; Carreira, B.; Pozzi, S.; Acúrcio, R.C.; Satchi-Fainaro, R.; Florindo, H.F.; Vicent, M.J. Current hurdles to the translation of nanomedicines from bench to the clinic. *Drug Deliv. Transl. Res.* **2022**, *12*, 500–525. [CrossRef] [PubMed]
4. Deng, H.; Liu, H.; Yang, Z.; Bao, M.; Lin, X.; Han, J.; Qu, C. Progress of selenium deficiency in the pathogenesis of arthropathies and selenium supplement for their treatment. *Biol. Trace Elem. Res.* **2022**, *200*, 4238–4249. [CrossRef] [PubMed]
5. Mojadadi, A.; Au, A.; Salah, W.; Witting, P.; Ahmad, G. Role for selenium in metabolic homeostasis and human reproduction. *Nutrients* **2021**, *13*, 3256. [CrossRef]
6. Garza-García, J.J.; Hernández-Díaz, J.A.; Zamudio-Ojeda, A.; León-Morales, J.M.; Guerrero-Guzmán, A.; Sánchez-Chiprés, D.R.; López-Velázquez, J.C.; García-Morales, S. The role of selenium nanoparticles in agriculture and food technology. *Biol. Trace Elem. Res.* **2022**, *200*, 2528–2548. [CrossRef]
7. Ikram, M.; Javed, B.; Raja, N.I. Biomedical potential of plant-based selenium nanoparticles: A comprehensive review on therapeutic and mechanistic aspects. *Int. J. Nanomed.* **2021**, *16*, 249–268. [CrossRef]
8. Ferro, C.; Florindo, H.F.; Santos, H.A. Selenium nanoparticles for biomedical applications: From development and characterization to therapeutics. *Adv. Healthc. Mater.* **2021**, *10*, 2100598. [CrossRef]
9. Wilson, T.; Temple, N.J.; Bray, G.A. *Nutrition Guide for Physicians and Related Healthcare Professions (Essential Minerals: Nutritional Requirements, Dietary Sources, and Deficiencies)*, 3rd ed.; Nutrition Guide for Physicians and Related Healthcare Professions (Nutrition and Health): 9783030825140: Medicine & Health Science Books @ Amazon.com; Springer: Berlin/Heidelberg, Germany, 2022; pp. 365–376.
10. Hashem, A.H.; Abdelaziz, A.M.; Attia, M.S.; Salem, S.S. Chapter 11, Selenium and Nano-Selenium-Mediated Biotic Stress Tolerance in Plants. In *Selenium and Nano-Selenium in Environmental Stress Management and Crop Quality Improvement*; Selenium and Nano-Selenium in Environmental Stress Management and Crop Quality Improvement (springer.com); Springer: Berlin/Heidelberg, Germany, 2022; pp. 209–226.
11. Laltlanmawia, C.; Saha, R.K.; Saha, H.; Biswas, P. Ameliorating effects of dietary mixture of *Withania somnifera* root extract and vitamin C in Labeo rohita against low pH and waterborne iron stresses. *Fish Shellfish. Immunol.* **2019**, *88*, 170–178. [CrossRef]
12. Khan Mohammad, K.R.; Khalili, M.B.; Sadeh, M.; Talebi, A.R.; Astani, A.; Shams, A. The effect of lipopolysaccharide from uropathogenic Escherichia coli on the immune system, testis tissue, and spermatozoa of BALB/c mice. *Clin. Exp. Reprod. Med.* **2021**, *48*, 105–110. [CrossRef]
13. Ahmed, M.M.; Hammad, A.A.; Orabi, S.H.; Elbaz, H.T.; Elweza, A.E.; Tahoun, E.A. Reproductive Injury in Male Rats from Acrylamide Toxicity and Potential Protection by Earthworm Methanolic Extract. *Animals* **2022**, *12*, 1723. [CrossRef] [PubMed]
14. Shahabadi, N.; Zendehcheshm, S.; Khademi, F. Selenium nanoparticles: Synthesis, in-vitro cytotoxicity, antioxidant activity and interaction studies with ct-DNA and HSA, HHb and Cyt c serum proteins. *Biotechnol. Rep.* **2021**, *30*, e00615. [CrossRef] [PubMed]
15. Shar, A.; Lakhan, M.; Wang, J.; Ahmed, M.; Alali, K.; Ahmed, R.; Ali, I.; Dayo, A. Facile synthesis and characterization of selenium nanoparticles by the hydrothermal approach. *Dig. J. Nanomater. Biostructures* **2019**, *14*, 867–872.
16. Ramamurthy, C.H.; Sampath, K.S.; Arunkumar, P.; Kumar, M.S.; Sujatha, V.; Premkumar, K.; Thirunavukkarasu, C. Green synthesis and characterization of selenium nanoparticles and its augmented cytotoxicity with doxorubicin on cancer cells. *Bioprocess Biosyst. Eng.* **2013**, *36*, 1131–1139. [CrossRef]
17. Anderson, R.; Moses, R.; Lenherr, S.; Hotaling, J.M.; Myers, J. Spinal cord injury and male infertility-a review of current literature, knowledge gaps, and future research. *Transl. Androl. Urol.* **2018**, *7*, S373–S382. [CrossRef]
18. Kim, C.R.; Noda, T.; Okada, Y.; Ikawa, M.; Baek, S.H. Protocol for isolation of spermatids from mouse testes. *STAR Protoc.* **2020**, *2*, 100254. [CrossRef] [PubMed]
19. Barrett, S.; De Franco, M.; Kellett, A.; Dempsey, E.; Marzano, C.; Erxleben, A. Anticancer activity, DNA binding and cell mechanistic studies of estrogen-functionalised Cu (II) complexes. *J. Biol. Inorg. Chem.* **2020**, *25*, 49–60. [CrossRef]

20. Prasad, K.S.; Patel, H.; Patel, T.; Patel, K.; Selvaraj, K. Biosynthesis of Se nanoparticles and its effect on UV-induced DNA damage. *Colloids Surf. B Biointerfaces* **2013**, *103*, 261–266. [CrossRef]
21. Abd El-Moneim, O.M.; Abd El-Rahim, A.H.; Hafiz, N.A. Evaluation of selenium nanoparticles and doxorubicin effect against hepatocellular carcinoma rat model cytogenetic toxicity and DNA damage. *Toxicol. Rep.* **2018**, *5*, 771–776. [CrossRef] [PubMed]
22. Kumaravel, T.S.; Vilhar, B.; Faux, S.P.; Jha, A.N. Comet assay measurements: A perspective. *Cell Biol. Toxicol.* **2009**, *25*, 53–64. [CrossRef]
23. Tice, R.R.; Agurell, E.; Anderson, D.; Burlinson, B.; Hartmann, A.; Kobayashi, H.; Miyamae, Y.; Rojas, E.; Ryu, J.C.; Sasaki, Y. Single cell gel/comet assay: Guidelines for in vitro and in vivo genetic toxicology testing. *Environ. Mol. Mutagen.* **2000**, *35*, 206–221. [CrossRef]
24. Burlinson, B. The in vitro and in vivo comet assays. In *Genetic Toxicology*; Springer: Berlin/Heidelberg, Germany, 2012; pp. 143–163. [CrossRef]
25. Rashid, T.M.; Nayef, U.M.; Jabir, M.S. Nano-ZnO decorated on gold nanoparticles as a core-shell via pulse laser ablation in liquid. *Optik* **2021**, *248*, 168164. [CrossRef]
26. Cittrarasu, V.; Kaliannan, D.; Dharman, K.; Maluventhen, V.; Easwaran, M.; Liu, W.C. Green synthesis of selenium nanoparticles mediated from Ceropegia bulbosa Roxb extract and its cytotoxicity, antimicrobial, mosquitocidal and photocatalytic activities. *Sci. Rep.* **2021**, *11*, 1032. [CrossRef] [PubMed]
27. Rahmah, M.I.; Sabry, R.S.; Aziz, W.J. Preparation of superhydrophobic Ag/Fe_2O_3/ZnO surfaces with photocatalytic activity. *Surf. Eng.* **2021**, *37*, 1320–1327. [CrossRef]
28. Alagesan, V.; Venugopal, S. Green synthesis of selenium nanoparticle using leaves extract of *Withania somnifera* and its biological applications and photocatalytic activities. *Bionanoscience* **2019**, *9*, 105–116. [CrossRef]
29. Galić, E.; Radić, K.; Golub, N.; Vitali Čepo, D.; Kalčec, N.; Vrček, E. Utilization of Olive Pomace in Green Synthesis of Selenium Nanoparticles: Physico-Chemical Characterization, Bioaccessibility and Biocompatibility. *Int. J. Mol. Sci.* **2022**, *23*, 9128. [CrossRef]
30. Ahmed, F.; Dwivedi, S.; Shaalan, N.M.; Kumar, S.; Arshi, N.; Alshoaibi, A.; Husain, F.M. Development of selenium nanoparticle-based agriculture sensor for heavy metal toxicity detection. *Agriculture* **2020**, *10*, 610. [CrossRef]
31. Pouri, S.; Motamedi, H.; Honary, S.; Kazeminezhad, I. Biological synthesis of selenium nanoparticles and evaluation of their bioavailability. *Braz. Arch. Biol. Technol.* **2018**, *60*, e170452. [CrossRef]
32. Habubi, N.; Bakr, N.; Salman, S. Optical parameters of amorphous selenium deposited by thermal evaporation technique. *Phys. Chem. Indian J.* **2013**, *8*, 54–58.
33. Panchal, S.; Chauhan, R. Variation in structural, electrical and optical properties of selenium nanowires after irradiation with Ni6+ ions. *Electron. Mater. Lett.* **2019**, *15*, 216–226. [CrossRef]
34. Jadhav, S.R.; Khairnar, U.P. Study of Optical Properties of Co-evaporated PbSe Thin Films. *Arch. Appl. Sci. Res.* **2012**, *4*, 169–177.
35. Almudhaffer, M.F.; Nattiq, M.A.; Jaber, M.A. Linear optical properties and energy loss function of Novolac: Epoxy blend film. *Arch. Appl. Sci. Res.* **2012**, *4*, 1731–1740.
36. Jiang, F.; Cai, W.; Tan, G. Facile synthesis and optical properties of small selenium nanocrystals and nanorods. *Nanoscale Res. Lett.* **2017**, *12*, 401. [CrossRef]
37. Gates, B.; Mayers, B.; Cattle, B.; Xia, Y. Synthesis and Characterization of Uniform Nanowires of Trigonal Selenium. *Adv. Funct. Mater.* **2002**, *12*, 219–227. [CrossRef]
38. Prasad, K.S.; Selvaraj, K. Biogenic synthesis of selenium nanoparticles and their effect on As (III)-induced toxicity on human lymphocytes. *Biol. Trace Elem. Res.* **2014**, *157*, 275–283. [CrossRef]
39. El-Nekeety, A.A.; Hassan, M.E.; Hassan, R.R.; Elshafey, O.I.; Hamza, Z.K.; Abdel-Aziem, S.H.; Hassan, N.S.; Abdel-Wahhab, M.A. Nanoencapsulation of basil essential oil alleviates the oxidative stress, genotoxicity and DNA damage in rats exposed to biosynthesized iron nanoparticles. *Heliyon* **2021**, *7*, e07537. [CrossRef]
40. Artimani, T.; Amiri, I.; Soleimani, S.; Saidijam, M.; Hasanvand, D.; Afshar, S. Amelioration of diabetes-induced testicular and sperm damage in rats by cerium oxide nanoparticle treatment. *Andrologia* **2018**, *50*, e13089. [CrossRef] [PubMed]
41. Onyeka, C.A.; Nwakanma, A.A.; Bakare, A.A.; Okoko, I.I.; Ofoego, U.C.; Wali, C.C.; Abengowe, F.C. Hypoglycemic, Antioxidant and Hepatoprotective Activities of Ethanolic Root Bark Extract of Chrysophyllum albidum in Alloxan-Induced Diabetic Rats. *Bangladesh J. Med. Sci.* **2013**, *12*, 298–304. [CrossRef]
42. Beji, R.S.; Rebey, I.B.; Jameleddine, S.; Ksouri, R. Assessment of the antidiabetic, antihyperlipidemic and antioxidant properties of Trigonella foenum-graecum Linnaeus, 1753 (Fenugreek) in alloxan-induced diabetic rats. *J. New Sci.* **2016**, *28*, 1602–1609.